Coupled versus uncoupled hindcast simulations of the Madden-Julian oscillation in the Year of Tropical Convection

Coupled versus uncoupled hindcast simulations of the Madden-Julian Oscillation in the Year of Tropical Convection

Ann Shelly,[1] Prince Xavier,[1] Dan Copsey,[1] Tim Johns,[1] José M. Rodríguez,[1]

Sean Milton[1] and Nicholas Klingaman[2]

Corresponding author: A. Shelly, Met Office, Fitzroy Rd, Exeter, Devon, EX1 3PB, UK (ann.shelly@metoffice.gov.uk)

[1]Met Office, Fitzroy Rd, Exeter, Devon

EX1 3PB,UK

[2]Department of Meteorology, University

of Reading, P.O. Box 243, Reading,

Berkshire RG6 6BB, UK

This study investigates the impact of a full interactive ocean on daily initialised 15 day hindcasts of the Madden Julian Oscillation (MJO), measured against a Met Office Unified Model (MetUM) atmosphere control simulation (AGCM) during a 3 month period of the Year of Tropical Convection (YOTC). Results indicate that the coupled configuration (CGCM) extends MJO predictability over that of the AGCM, by up to 3-5 days. Propagation is improved in the CGCM, which we partly attribute to a more realistic phase relationship between sea surface temperature (SST) and convection. In addition, the CGCM demonstrates skill in representing downwelling oceanic Kelvin and Rossby waves which warm SSTs along their trajectory, with the potential to feed back on the atmosphere. These results imply that an ocean model capable of simulating internal ocean waves may be required to capture the full effect of air-sea coupling for the MJO.

1. Introduction

The MJO [*Madden and Julian*, 1971] is the leading mode of intraseasonal variability in the tropics. It exerts considerable influence on tropical weather and climate variability, such as the Indian and Asian monsoons [*Goswami*, 2005; *Hsu*, 2005; *Wheeler and McBride*, 2005] and tropical cyclone activity [*Vitart*, 2009], and can modulate extratropical weather patterns through forcing of atmospheric Rossby waves by the divergent outflow from tropical convection which propagate towards the mid latitudes [*Ferranti et al.*, 1990; *Cassou*, 2008].

It has been demonstrated the forecast skill of MJO improves in atmospheric simulations if forced with high temporal frequency SST variability and such simulations also display better rainfall variability [*Klingaman et al.*, 2008; *Matthews*, 2004]. The importance of 2-way interaction between atmosphere and ocean components in models [*Woolnough et al.*, 2007; *Fu et al.*, 2013] has also been suggested. Another potentially important aspect in successfully simulating the MJO in models is maintaining a correct phase relationship in the atmospheric response to SST anomalies [*Kim et al.*, 2010; *Fu et al.*, 2007].

Evidence is increasing that suggests ocean models may be necessary to capture dynamical ocean feedbacks important for initialising and maintaining the MJO. *Webber et al.* [2010, 2012] highlight the important role of ocean dynamics particularly in the Indian Ocean, where a tropical ocean internal wave response to the MJO leads to SST anomalies with the potential to feed back on the atmosphere and trigger further MJO events. Anomalous easterlies in the equatorial Indian Ocean can act to force a westward propagating downwelling (upwelling) Rossby wave and SST increases (decreases) in phase with

the passage of the wave [*Seiki et al.*, 2013; *Shinoda et al.*, 2013].*Drushka et al.* [2012] demonstrate that mixed layer depth variations on MJO time scales modulate the heat budget by 40% in the warm pool region. These studies imply that to accurately model the MJO, ocean dynamics may need to be simulated adequately enough to resolve internal waves as well as SST anomalies forced by waves. Developing a better picture for how MJO forcing impacts the ocean, and how this may feed back onto the MJO, is necessary for improving MJO prediction and modelling.

This study extends previous work by carrying out daily initialised MJO simulations with a global coupled MetUM configuration and by using a more complex ocean model than has been previously applied to MJO and air-sea interactions investigations on medium range timescales. The experimental setup, outlined in section 2 permits us to examine the influence of the sub-surface ocean on MJO simulations. As MetUM uncoupled operational forecast models already have a good general representation of the MJO on these timescales [*Gottschalck et al.*, 2010], we consider the model a suitable tool for analysing the impact of 2-way air-sea coupling on mechanisms instrumental in the lifecycle and predictability of the MJO.

2. Data and Methods

We compare MetUM models for a set of daily initialized 15 day hindcasts with observation and analysis data, for the period falling within the Year of Tropical Convection (YOTC). Two strong MJO episodes denoted as YOTCE (15 October - 6 Dec 2009) and YOTCF (16 Dec 2009 - 29 Jan 2010) with reference to Figure 3 of *Waliser and Coauthors* [2012] form the central focus for our analysis.

The models used are a MetUM CGCM and a corresponding AGCM with prescribed ocean boundary conditions using persisted SST anomalies. Anomalies in the MetUM analysis are calculated relative to Hadley Centre Sea Ice and Sea Surface Temperature data set (HadISST) climatology [*Rayner et al.*, 2003]. The anomaly is added to the evolving climatological cycle of SST on a daily basis to obtain the AGCM SST forcing. We persist SST anomalies instead of persisting initial SSTs as the seasonal cycle affects the amplitude of SSTs within a few days, indicated by sensitivity tests carried out at the Met Office.

The atmospheric model physics is based on the GlobalAtmos3.0 version [*Walters and Coauthors*, 2011], at a resolution of 60km in the horizontal with 85 vertical levels. The ocean component is based on Nucleus for European Modelling of the Ocean (NEMO) configured with version 3.2 physics on a 0.25° horizontal grid, with 75 vertical levels and 1m vertical resolution in the top 10m, coupled to the The Los Alamos sea ice model (CICE). The atmosphere is initialised from MetUM analyses,the ocean component is initialised from NEMOVAR (NEMO VARiational data assimilation system) analyses [*Mogensen et al.*, 2009] and the models communicate on a 3 hourly coupling frequency. Any difference in hindcast skill in the CGCM compared to AGCM measures the impact of 2-way air-sea interaction between the model components in dynamically predicting SSTs.

In order to measure MetUM performance and ability to represent processes key to the MJO, a number of metrics are calculated. This study focuses on dates which contain an MJO in the initial conditions; it does not include hindcasts from prior to the start of the MJO events. RMM1 and RMM2 are formed following the Wheeler and Hendon

(*Wheeler and Hendon* [2004]; hereinafter WH) method, removing the annual mean and the first 3 harmonics of the annual cycle. Anomalies of Outgoing Longwave Radiation (OLR), and winds at 850hPa (u850) and 200hPa (u200) are combined and projected onto WH empirical orthogonal functions to yield real time multivariate time series RMM1 and RMM2. Anomaly correlations are calculated against MetUM operational analysis following the method of *Gottschalck et al.* [2010], as a measure of MJO predictability in both model configurations. Significance of the correlation coefficients are tested using the Pearson critical value table. The sample sizes for YOTCE and YOTCF are 50 and 44, respectively.

We are interested in relationships which exist between the atmosphere and ocean and the method of time lagged correlations is used to examine the forcing of the atmosphere by the ocean and vice versa. The model data was regridded to a 2.5° x 2.5° grid, to match NOAA OLR observations. A band pass filter is commonly used to isolate the MJO related signal between 30-80 days in longer simulations, but it is not possible to apply this technique to 15 day hindcasts as the band pass length exceeds hindcast length. Instead, to minimise high frequency variability prior to calculating lagged relationships, a 5 day running mean is applied to the data. Either side of each 15 day hindcast is padded with MetUM analyses data, a viable technique at the beginning of the hindcast when model fields are close to initial conditions, but we acknowledge that the end of the hindcast will likely erroneously improve due to influence of the analysis. Therefore, we disregard hindcast data past day 13 that has been treated in this manner. This smoothing has only been applied to data used in figure 2.

The lagged phase relationship between SST and convection is calculated, using OLR as a proxy for convection. A single 15 day initialised hindcast does not provide a sufficiently long timeseries to adequately assess lagged relationships. To circumvent this issue, we collect all of the day 5 lead times from each 15 day hindcast over the YOTCE and (separately) YOTCF period. We extract the Indian Ocean region from the full global dataset and average over latitudes between 10°N and 10°S, for each point of longitude between 60°E-100°E between the SST and OLR datasets. We subsequently perform lagged correlations between the datasets for lags of up to 15 days. At each longitude, the latitude-averaged OLR is lag correlated with the latitude-averaged SST, for leads and lags up to 15 days. NOAA OLR [*Liebmann and Smith*, 1996] observations and operational sea surface temperature and sea ice analyses (OSTIA) [*Donlon et al.*, 2012] are used to verify the data. Previous work [*Klingaman et al.*, 2011] suggests that correlations between these fields peak at a 10 day lag (see supplementary plot). In order to examine propagation of each YOTC event, we additionally calculate lagged correlations of OLR at a base point(70°E) with latitude-averaged OLR at all points of longitude in the Indian Ocean.

Chelton et al. [2003] demonstrated that Rossby waves generally have a sea surface height (SSH) maxima centred 4 degrees of latitude away from the equator, with positive (negative) SSH anomalies associated with a downwelling (upwelling) Rossby wave. To assess the modelled representation of tropical ocean waves associated with the MJO, we examine anomalies of both SSH and depth of the 20C isotherm (Dep20) and verify against daily Forecast Ocean Assimilation Model (FOAM) analyses [*Storkey et al.*, 2010] for these quantities. We validated the daily SSH FOAM analysis against Archiving Validation and

Interpretation of Satellite Oceanographic Data (AVISO) observations and these largely agree (not shown). To search for propagating Rossby waves, we form a latitudinal average between 2°N-8°N and 2°S-8°S in the Indian Ocean and plot time longitude diagrams for the period spanning Sept 2009 to Jan 2010 for analyses and CGCM hindcasts at day 1 and day 14. To study equatorial Kelvin wave propagation, a latitudinal average is formed over the equatorial wave guide between 2°N-2°S in the Indian Ocean.

3. Results

During YOTCE, the CGCM demonstrates enhanced performance for RMM1 over that of the AGCM from day 4 for combined fields, extending predictability by 3 days based on a threshold of 0.6 (Fig. 1, left). The configurations display similar skill out to day 11 for RMM2, after which the CGCM is slightly more skilful. The persistence hindcast is shown to rapidly diverge from the dynamical hindcasts at day 1, indicating a rapid loss of predictability. Over YOTCF, the AGCM has greater RMM1 predictability from day 5 out to day 10, after which the score rapidly deteriorates. CGCM anomalies remain above a correlation of 0.6 in these later lead times (Fig. 1, right) and extends predictability by 5 days in the case of RMM1 for combined fields based on a threshold of 0.6. However, both configurations are similar in the case of RMM2.

CGCM correlation scores for OLR are demonstrably better than the AGCM for both RMM1 and RMM2. Over the YOTCE period, the CGCM shows greater performance from day 8 (RMM1) and from day 4 (RMM2) and similarly for the YOTCF event, from day 6 (RMM1) and day 8 (RMM2). Performance is comparable for upper level winds as the two configurations remain close throughout lead times. Nonetheless, the CGCM displays

a slight improvement over YOTCE, particularly for RMM2 and for RMM1 between days 12-15. In the case of U850, the CGCM shows generally greater predictability in the latter 5 days for YOTCF but similar performance over YOTCE. In general, the CGCM has greater predictability particularly for OLR and U850 and is capable of maintaining higher correlation scores over the entire hindcast length. The results for both simulations are found to be mostly significantly different from zero (denoted as triangles in Fig.1) but the differences between the two simulations are not found to be significant. We acknowledge that the study is somewhat limited by focusing on deterministic hindcasts of two MJO events and would expect some variation in evolution and characteristics between MJO events.

We next examine possible mechanisms leading to the improved predictability seen in the CGCM hindcasts. Propagation of the convective centre of action of the MJO through the Indian Ocean over YOTCE is illustrated in Fig. 2 (a-c). The eastward propagation of the MJO is apparent in the observations throughout the period (Fig 2.a). As the main centre of convection follows a trajectory across the Indian Ocean and clear skies (positive OLR) turn cloudy (negative OLR), the correlations switch sign from negative to positive. The AGCM simulated MJO is stationary by day 5 (Fig 2.c). Lead-lag correlations as shown in Fig.2b for day 5, but constructed using respectively later days in the hindcast, indicate that the CGCM is still able to propagate the MJO out to day 9 hindcasts, though slower than observed (not shown). This result indicates that dynamically evolving SSTs play a role in improving propagation of the MJO and is corroborated by other studies [*Fu et al.*, 2007; *Waliser et al.*, 1999].

The lack of propagation of the MJO in the AGCM after a few days could be related to a loss of coherent evolution between atmospheric convection and underlying SST anomalies related to the MJO [*Waliser et al.*, 1999; *Klingaman et al.*, 2011]. In figure 2(d-f), the SST-convection relationship is investigated through calculation of the lagged correlation between OLR and SST anomalies. Figure 2 (e & f) depict the lagged correlation coefficients in the Indian Ocean for all day 5 hindcasts for the CGCM and AGCM for YOTCE. Similar results are obtained for YOTCF and in the Western Pacific (not shown). Observed warm SSTs are shown to lead enhanced convection by 5-10 days and conversely, active convection leads cool SSTs by 5-10 days (Fig 2.d). The CGCM reproduces the observed phase relationship, though it is slightly weaker and maintains the relationship out to day 13 lead time (not shown). However, in the AGCM experiment, convection adjusts to a location where SST anomalies peak, which results in co-located OLR and SST anomalies by day 5. In reality, warm SST anomalies not only influence the convection but are concurrently influenced by the atmospheric state. The AGCM is unable to reproduce this key air-sea interaction and the MJO simulation suffers. A phase relationship analysis of operational global MetUM and climate model configurations is presented in supplementary material which corroborates results presented here.

Fu et al. [2013] found that an AGCM forced by daily observed SSTs can sustain the SST-convection relationship and that the match between the atmospheric MJO conditions and underlying SST is the important factor. However, this is not practical from an operational forecasting standpoint when the future evolution of the SST is unknown. Thus the only

way that this mechanism can be represented to the advantage of operational forecasting, is through an interactive ocean.

It is clear from Figure 2 that that SST modulates and is modulated by the MJO. We next consider the CGCM representation of tropical ocean waves, which play a role in modulating the SST in the tropical warm pool [*Mccreary*, 1983; *Shinoda*, 2005]. Downwelling waves deepen the thermocline and raise the SST by reducing entrainment of cold sub-surface waters, while upwelling waves lead to enhanced entrainments and cooling. *Suryachandra et al.* [2012] demonstrate through a budget analysis that advection plays a key role in warming SSTs in the region, suggesting that it is important that tropical waves are well simulated in a GCM.

Enhanced convection and strong surface winds likely associated with the MJO YOTCE activity in mid October excites an oceanic Kelvin wave which propagates eastward along the equator (Fig. 3a) reaching the Maritime Continent in late November, visible as a positive anomaly moving eastward in the FOAM analysis Dep20 field. The perturbation in the ocean height (equatorial SSH, not shown) and at the thermocline (Dep20) is well reproduced in CGCM day 1 and day 14 hindcasts, with a propagation speed and amplitude similar to the FOAM analysis (Fig 3.b,c). The modelled OLR is similar to observed OLR anomalies at day 1 (Fig 3.b, contours) in magnitude and propagation but appears stationary by day 14 (Fig 3.c).

Several westward propagating, downwelling Rossby waves are noticeable over the period between Oct 2009 and Jan 2010 (R1-R3). R1 propagates west from 65°E between Sept and early November (Fig 3.d), R2 moves from 90°E to 60°E between Sept and January.

The third observed wave (R3) is triggered in late November coinciding with YOTCE MJO propagation into the Maritime Continent and moves west from early December towards 80°E by mid January. A potential mechanism for the trigger of R3 could be through reflection and splitting of the earlier Kelvin wave back into the Indian Ocean along the Rossby wave guide at 4°N/S [*Chelton et al.*, 2003].

Though SST is sensitive to many processes and the daily SST anomaly field will contain high frequency variability caused by surface fluxes and the diurnal cycle; there are clearly some westward propagating SST anomalies which follow the trajectory of the westward propagating Rossby waves (Fig 3.g). The R1 wave seen in the SSH propagates westward at the same speed and direction as a warm SST anomaly seen in the OSTIA dataset (Fig 3.g). It is possible that this wave could have had warmed SSTs prior to YOTCE, creating conditions more amenable to large-scale convection. Competing processes clearly play a role and the prominent SST cooling caused by the passage of the YOTCE and YOTCF events is visible in the anomalously cool conditions in mid November and again in late December. Warming induced by the passage of R2 is likely overshadowed by entrainment of deeper, cooler waters brought about by strong winds and large scale convection associated with the MJO event moving through the Indian Ocean. However, it does appear that there is westward propagation of positive SST anomalies superimposed on top of this pattern (Fig 3.g). This is particularly obvious as a break in the eastward propagation of cool SST anomalies between 15-25 November, where the anomalies briefly turn slightly positive for about 10 days. Again in the case of R3, there is an indication of westward motion of warm SSTs. The CGCM captures all 3 Rossby waves and the SST anomaly

fields largely resemble the OSTIA analysis. The influence of data assimilation is likely to be large on the initial days of the hindcast (Fig. 3h), however SSH and SST anomalies for day 14 hindcasts still retain resemblance to the analyses (Fig. 3.f,i). Warm SSTs advected by the tropical waves could potentially act as a positive feedback onto further convective events. *Webber et al.* [2012] showed that MJO events can coincide with the arrival of a downwelling oceanic equatorial Rossby wave in the western Indian Ocean, implying that such waves could act as a trigger.

4. Conclusions

Our findings indicate that an interactive ocean produces improved MJO hindcasts over those of an AGCM forced with persisted SST anomalies. It is clear that there is potential for SST anomalies to be a key component of the MJO. Skill measures are improved in the CGCM likely because of the dynamical prediction of SSTs. We have not considered the complex impact of drift in the mean state of the CGCM on MJO hindcasts here, as SSTs in the Indian Ocean display minimal drift by day 14 over YOTCE/F (not shown). *Klingaman and Woolnough* [2014] address the separation of climate mean state influence on MJO simulation from improvements due to coupled processes in the Met Office Hadley Centre model and we will address contributions from SST drifts on NWP timescales in future work. We have demonstrated that the propagation of the MJO suffers in the AGCM simulation, which could result from the failure to represent the phase relationship that exists between convection and SST. The CGCM shows skill in representation of both oceanic equatorial Kelvin waves and of westward propagating Rossby waves out to 15 days. It has also been shown that while SST is sensitive to many different processes,

anomalously warm waters occur along the trajectory of downwelling tropical waves and this process could be important to the lifecycle of the MJO. The case for using an ocean model capable of simulating waves seems strong, given that tropical waves appear both to influence and be influenced by the MJO.

Acknowledgments. The authors wish to thank Pat Hyder for useful advice and two anonymous reviewers for their constructive comments which have helped to improve this work. This work is supported by the Joint DECC/DEFRA Met Office Hadley Centre Climate Programme (GA01101). Data used to generate figures is available via contacting the lead author.

References

Cassou, C. (2008), Intraseasonal interaction between the Madden-Julian Oscillation and the North Atlantic Oscillation, *Nature*, *455*(7212), 523–527.

Chelton, D., M. Schlax, J. Lyman, and G. Johnson (2003), Equatorially trapped Rossby waves in the presence of meridionally sheared baroclinic flow in the Pacific Ocean, *Prog. Oceanog.*, *56*(2), 323–380.

Donlon, C. J., M. Martin, J. Stark, J. Roberts-Jones, E. Fiedler, and W. Wimmer (2012), The Operational Sea Surface Temperature and Sea Ice Analysis (OSTIA) system, *Remote Sens. Env.*, *116*(SI), 140–158.

Drushka, K., J. Sprintall, S. T. Gille, and S. Wijffels (2012), In Situ Observations of Madden-Julian Oscillation Mixed Layer Dynamics in the Indian and Western Pacific Oceans, *J. Clim.*, *25*(7), 2306–2328.

Ferranti, L., T. Palmer, F. Molteni, and E. Klinker (1990), Tropical extratropical interaction associated with the 30-60 day oscillation and its impact on medium and extended range prediction, *J. Atmos. Sci.*, *47*(18), 2177–2199.

Fu, X., B. Wang, D. E. Waliser, and L. Tao (2007), Impact of atmosphere-ocean coupling on the predictability of monsoon intraseasonal oscillations, *J. Atmos. Sci.*, *64*(1), 157–174.

Fu, X., J.-Y. Lee, P.-C. Hsu, H. Taniguchi, B. Wang, W. Wang, and S. Weaver (2013), Multi-model MJO forecasting during DYNAMO/CINDY period, *Clim. Dyn.* , *41*(3-4), 1067–1081.

Goswami, B. (2005), South Asian Monsoon, in *Intraseaonal Variability in the Atmosphere-Ocean Climate System*, edited by W. Lau and D. Waliser, pp. 19–55, Praxis Publishing.

Gottschalck, J., M. Wheeler, K. Weickmann, F. Vitart, N. Savage, H. Lin, H. Hendon, D. Waliser, K. Sperber, M. Nakagawa, C. Prestrelo, M. Flatau, and W. Higgins (2010), A framework for assessing operational Madden-Julian Oscillation forecasts: A CLIVAR MJO Working Group Project, *Bull. Am. Meteorol. Soc.*, *91*(9), 1247–1258.

Hsu, H. (2005), East Asian Monsoon, in *Intraseaonal Variability in the Atmosphere-Ocean Climate System*, edited by W. Lau and D. Waliser, pp. 63–90, Praxis Publishing.

Kim, H.-M., C. D. Hoyos, P. J. Webster, and I.-S. Kang (2010), Ocean-atmosphere coupling and the boreal winter MJO, *Clim. Dyn.*, *35*(5), 771–784.

Klingaman, N., and S. Woolnough (2014), The role of air-sea coupling in the simulation of the Madden-Julian Oscillation in the Hadley Centre Model, *Q.J.R. Meteorol. Soc.*, doi:10.1002/qj.2295.

Klingaman, N. P., P. M. Inness, H. Weller, and J. M. Slingo (2008), The Importance of High-Frequency Sea Surface Temperature Variability to the Intraseasonal Oscillation of Indian Monsoon Rainfall, *J. Clim.*, *21*(23), 6119–6140.

Klingaman, N. P., S. J. Woolnough, H. Weller, and J. M. Slingo (2011), The Impact of Finer-Resolution Air-Sea Coupling on the Intraseasonal Oscillation of the Indian Monsoon, *J. Clim.*, *24*(10), 2451–2468.

Liebmann, B., and C. Smith (1996), Description of a Complete (Interpolated) Outgoing Longwave Radiation Dataset, *Bull. Am. Meteorol. Soc.*, *77*, 1275–1277.

Madden, R. A., and P. R. Julian (1971), Detection of a 40-50 day oscillation in the zonal wind in the tropical Pacific, *J. Atmos. Sci.*, *28*(5), 702–708.

Matthews, A. (2004), Atmospheric response to observed intraseasonal tropical sea surface temperature anomalies, *Geophys. Res. Lett.*, *31*(14).

Mccreary, J. (1983), A model of tropical ocean atmosphere interaction, *Mon. Weather Rev.*, *111*(2), 370–387.

Mogensen, K., M. Balmaseda, A. Weaver, M. Martin, and A. Vidard (2009), NEMOVAR: A variational data assimilation system for the NEMO ocean model, *ECMWF newsletter*.

Rayner, N., D. Parker, E. Horton, C. Folland, L. Alexander, and D. Rowell (2003), Global analyses of sea surface temperature, sea ice, and night marine air temperature since the late nineteenth century, *J.Geophys.Res*, *108*(D14).

Seiki, A., M. Katsumata, T. Horii, T. Hasegawa, K. J. Richards, K. Yoneyama, and R. Shirooka (2013), Abrupt cooling associated with the oceanic rossby wave and lateral advection during cindy2011, *J.Geophys.Res.-Oceans*, *118*(10), 333–358.

Shinoda, T. (2005), Impact of the diurnal cycle of solar radiation on intraseasonal SST variability in the western equatorial Pacific, *J. Clim.*, *18*(14), 5523-5535.

Shinoda, T., T. Jensen, M. Flatau, and S. Chen (2013), Surface Wind and Upper-Ocean Variability Associated with the Madden Julian Oscillation Simulated by the Coupled Ocean Atmosphere Mesoscale Prediction System (COAMPS), *Mon. Weather Rev.*, *141*, 2290–2307.

Storkey, D., E. W. Blockley, R. Furner, C. Guiavarc'h, D. Lea, M. J. Martin, R. M. Barciela, A. Hines, P. Hyder, and J. R. Siddorn (2010), Forecasting the ocean state using NEMO:The new FOAM system, *J. Oper. Ocean.*, *3*(1), 3–15.

Suryachandra, A., R. Dhakate, S. Saha, S. Mahapatra, H. Chaudhari, S. Pokhrel, and S. Sahu (2012), Why is Indian Ocean warming consistently?, *Climatic Change*, *110*(3-4), 709–719.

Vitart, F. (2009), Impact of the Madden Julian Oscillation on tropical storms and risk of landfall in the ECMWF forecast system, *Geophys. Res. Lett.*, *36*.

Waliser, D., K. Lau, and J. Kim (1999), The influence of coupled sea surface temperatures on the Madden-Julian oscillation: A model perturbation experiment, *J. Atmos. Sci.*, *56*(3), 333–358.

Waliser, D. E., and Coauthors (2012), The year of tropical convection (may 2008-april 2010): climate variability and weather highlights, *Bull. Am. Meteorol. Soc.*, *93*, 1189–1218.

Walters, D. N., and Coauthors (2011), The Met Office Unified Model Global Atmosphere 3.0/3.1 and JULES Global Land 3.0/3.1 configurations, *G.M.D.*, *4*(4), 919–941.

Webber, B. G. M., A. J. Matthews, and K. J. Heywood (2010), A dynamical ocean feedback mechanism for the Madden-Julian Oscillation, *Q.J.R. Meteorol. Soc.*, *136*(648, A), 740–754.

Webber, B. G. M., A. J. Matthews, K. J. Heywood, and D. P. Stevens (2012), Ocean Rossby waves as a triggering mechanism for primary Madden-Julian events, *Q.J.R. Meteorol. Soc.*, *138*(663, B), 514–527.

Wheeler, M., and H. Hendon (2004), An all-season real-time multivariate MJO index: Development of an index for monitoring and prediction, *Mon. Weather Rev.*, *132*(8), 1917–1932.

Wheeler, M., and J. McBride (2005), Australian-Indonesian Monsoon, in *Intraseaonal Variability in the Atmosphere-Ocean Climate System*, edited by W. Lau and D. Waliser, pp. 125–168, Praxis Publishing.

Woolnough, S. J., F. Vitart, and M. A. Balmaseda (2007), The role of the ocean in the Madden-Julian Oscillation: Implications for MJO prediction, *Q.J.R. Meteorol. Soc.*, *133*(622, A), 117–128.

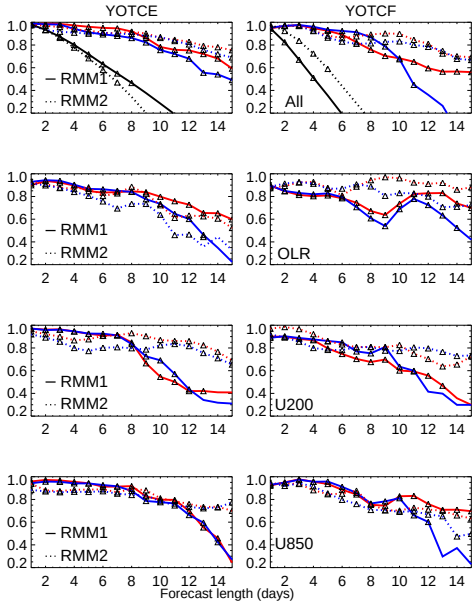

Figure 1. Hindcast anomaly correlation scores during YOTCE(left) and YOTCF(right) for combined fields (top), OLR (2nd from top), U200 (3rd from top) and U850(bottom) as measured against MetUM analyses, for MJO amplitudes exceeding 1.All phases are included in each plot. The CGCM is in red and AGCM in blue. A persistence hindcast (black) is shown for combined fields. Significance at 99% level is denoted by a triangle.

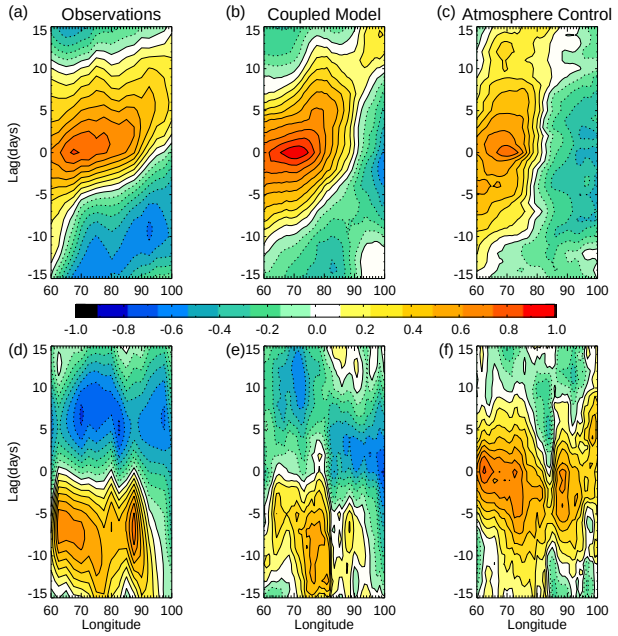

Figure 2. Lead-lag correlations for OLR at a base point of 70°E with OLR at all points of longitude in the Indian Ocean over YOTCE period [15 Oct-6 Dec 2009] for: (a) observations (b) CGCM and (c) AGCM, for all day 5 hindcasts. Lead-lag correlations over YOTCE period [15 Oct-6 Dec 2009] for SST correlated with OLR in the Indian Ocean for (d) observations, (e) CGCM hindcast and (f) AGCM hindcast(surface temperature at sea points), for all day 5 hindcasts.

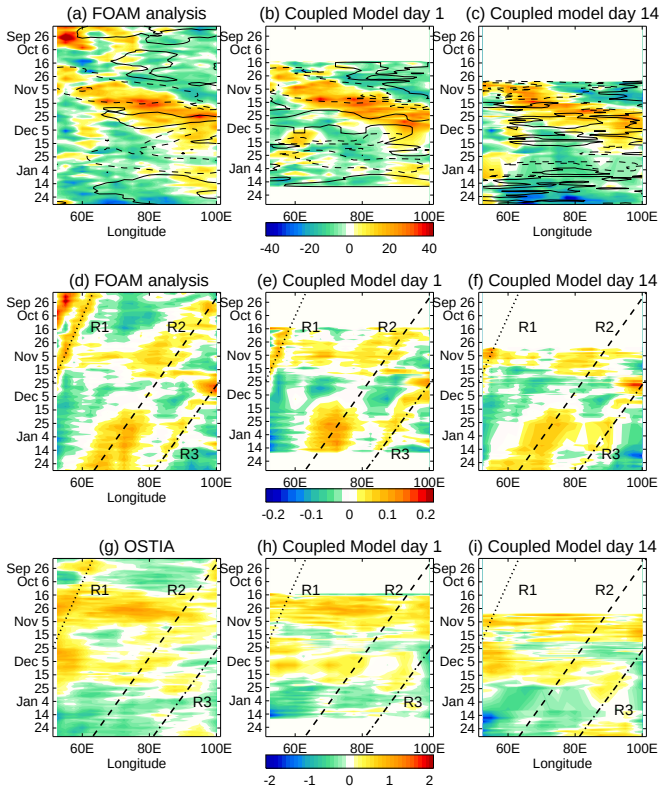

Figure 3. Time-longitude plots for (Top) Dep20 anomaly(m) and OLR anomaly (+/-10 Wm-2) for (a) FOAM analysis(shading) and NOAA OLR (contours) (b) day 1 CGCM hindcasts and (c) day 14 CGCM hindcasts averaged between 2°N-2°S; (Middle) SSH anomaly (m) for (d)FOAM analysis (e) day 1 CGCM hindcasts and (f) day 14 CGCM hindcasts averaged between 2°N-8°N and 2°S-8°S.; (Bottom) SST anomaly field for (g) OSTIA (h) day 1 CGCM hindcasts and (i) day 14 CGCM hindcasts averaged between 2°N-8°N and 2°S-8°S. Diagonal lines (R1,R2,R3) in (d)-(i) represent downwelling Rossby waves propagating from East to West across the Indian Ocean.